MTPA Cooperative Control Strategy of Double Stator DC-Bias Hybrid Excitation Machine Considering Inductance Nonlinearity

Han Yi, Yiming Fan, Yuting Lu, *Graduate Student Member, IEEE*, Guodong Feng, *Senior Member, IEEE*, and Liangliang Wei, *Member, IEEE*

***Abstract*—This article proposes a maximum torque per ampere (MTPA) cooperative control strategy for a double stator dc-bias hybrid excitation machine (DS-HEM) considering inductance nonlinearity. The proposed DS-HEM uses integrated windings and double stators to improve the torque density, efficiency, and flux regulation capability. Moreover, the proposed MTPA cooperative control strategy considering inductance nonlinearity can achieve high torque and lower copper loss. First, the configuration and drive system of the proposed machine is introduced and a mathematical model of the proposed machine is established, then the proposed MTPA cooperative control strategy considering two dimensions of the armature current and dc-bias current is calculated by using the Lagrange extremum method. Besides, the inductance nonlinearity is also considered by establishing the quadratic polynomial model. Finally, a prototype of the proposed machine is fabricated, and various experiments are conducted to validate the accuracy and effectiveness of the proposed method. Compared with conventional current control strategies, the proposed MTPA cooperative control strategy can generate a larger output torque and lower copper loss.**

***Index Terms*—Cooperative control strategy, DC bias, hybrid excitation, inductance nonlinearity, maximum torque per ampere (MTPA).**

I. Introduction

PERMANENT magnet synchronous motors (PMSM) have attracted more and more attention because of their high efficiency, high power density, and high torque density. Due to these advantages, PMSM is widely used in electric vehicles and other industrial applications [1], [2], [3], [4]. However, since the excitation source of traditional PMSM is only a permanent magnet, the air-gap magnetic field is difficult to adjust. Thus, the speed adjust range is limited. To improve the speed range of the motor, many scholars have begun to research hybrid excitation machines (HEMs) [5]. Compared with the traditional PMSM, an HEM is equipped with a set of field winding to generate additional electric excitation fields, so the air-gap magnetic field and speed range can be flexibly adjusted by changing the current in the field winding [6], [7], [8], [9].

Nonetheless, the additional field winding still occupies the stator space and increases the copper loss, to reduce the efficiency. To eliminate space conflicts and improve efficiency, the concept of integrated windings is introduced to the HEMs [10]. Various new topologies with integrated windings have been proposed in [11] and [12]. In [13], a permanent magnet machine with dc-bias current is proposed, but the auxiliary tooth in the stator may lead to low efficiency. In [14], a split-tooth stator permanent magnet vernier machine with zero-sequence current excitation is proposed to enhance the torque density and flux adjustment capability, but the PM and armature winding suffer from space conflicts. In [15], a hybrid excitation doubly salient machine with a double stator is proposed. The Halbach PM arrays and integrated windings are utilized to improve the torque density and also widen the speed region correspondingly. Deriving from the machine in [15], a double-stator HEM with dc-bias current is proposed in [16], which adopts the dc-bias sinusoidal current and consequent-pole PM to promote flux regulation capability, whereas the torque density and efficiency are not high enough.

Compared with traditional PMSM, the HEM should control the excitation current as a new dimension. Consequently, the HEM can be controlled by two dimensions of excitation current and armature current, and the control method is more flexible. In [17], a current control strategy for an axial-parallel HEM with an auxiliary winding is proposed, the field current and armature current can both be decreased because the auxiliary winding couples with the PM flux and suppresses phase voltage. Nonetheless, the auxiliary winding leads to the increased complexity of the drive circuit. In [18], a cooperative control method of minimum copper loss for a hybrid excitation double salient machine is proposed, and the optimal efficiency can be obtained when the copper consumption of armature winding and excitation winding are equal. In [19], a control method of minimum copper consumption per unit torque in full speed

Received 29 August 2024; revised 28 November 2024; accepted 15 January 2025. Date of publication 27 January 2025; date of current version 26 February 2025. This work was supported in part by the National Natural Science Foundation of China under Grant 62203478, in part by the Natural Science Foundation of Guangdong Province under Grant 2024A1515011234, and in part by Fundamental Research Funds for the Central Universities, Sun Yat-sen University, under Grant 24qnpy167. Recommended for publication by Associate Editor K. Basu. *(Corresponding author: Liangliang Wei.)*

The authors are with the School of Intelligent Systems Engineering, Sun Yat-sen University, Shenzhen 518107, China (e-mail: yihan@mail2.sysu.edu.cn; fanym6@mail2.sysu.edu.cn; luyt28@mail2.sysu.edu.cn; fenggd6@mail.sysu.edu.cn; weilliang@mail.sysu.edu.cn).

Color versions of one or more figures in this article are available at https://doi.org/10.1109/TPEL.2025.3534830.

Digital Object Identifier 10.1109/TPEL.2025.3534830

domain for a hybrid excitation flux switching motor is proposed, which ensures optimal copper consumption per unit output torque through reasonable distribution of armature current and excitation current. In [20], a current region control strategy with a wide speed range of a consequent-pole HEM is proposed to achieve multimode operation capability. However, the existing studies mainly focus on the control method with additional field winding, and the control strategy with integrated windings lacks consideration.

For the HEM that uses integrated windings, as the control circuit needs to use the dual three-phase inverter, the control method would be more complicated. In [21], the effects of the proportion of different dc-bias currents to the total current on the machine torque, power factor, and efficiency are investigated, which verifies that dc-bias current plays an important role in the dc-bias HEM. Nonetheless, the specific current distribution strategy is not considered. In [22], the influence of the dc-bias current ratio on the speed range is studied, indicating that the utilization of dc-bias current and d-axis current can broaden the speed range. However, the loss of the machine is not considered, and the efficiency of the machine can be further enhanced. When the machine is operated at the constant torque region, the maximum torque per ampere (MTPA) current control strategy is generally used. The traditional MTPA control method adopts the current distribution strategy based on $i_d = 0$ and $i_q = \sqrt{2}i_0$ [23], which is easy to realize, but the excitation current is not considered as an extra dimension, thereby it cannot achieve the optimal performance. In [24], an MTPA control strategy for dc-bias HEM is proposed, which performs the polynomial fitting on the optimal current ratio obtained in the experiments, but the nonlinear inductance is not considered and may not achieve optimal results for different current proportions. In [25], an MTPA control strategy for dc-bias HEM is proposed, which uses the MTPA control law and virtual signal injection to achieve accurate MTPA operation and rapid dynamic magnetization capability, but the inductance modeling considering the armature and excitation currents is not considered. Therefore, the control strategy of dc-bias HEMs from two dimensions of armature and excitation currents still needs further research.

In addition, to control the HEM efficiently and accurately, it is vital to establish the model of the HEM accurately. In [26], a mathematical model of a dc-bias vernier reluctance machine is built, and the voltage equation and torque equation of the machine are derived under the $dq0$-frame, but it is not suitable for HEMs as PM is not used in the machine. For HEMs, the electric magnetic field and the permanent magnetic field are coupled, and the model of HEMs is more complex. In [27], an equivalent mathematical model of a hybrid excitation flux switching machine in the dq coordinate system is established based on rotor field orientation. In [28], a multi-dq axis mathematical model of a novel alternating-pole HEM is established based on the equivalent air gap model, which aims to solve the problem of air gap asymmetry affecting the modeling. For HEMs that use integrated windings, the coupling of ac and dc flux is more complex. In [29], the mathematical model of a hybrid excited vernier reluctance machine is established in the dq coordinate system, but the coupling between the dc component and the armature component is not considered. Hence, the modeling of dc-bias HEMs should be further studied.

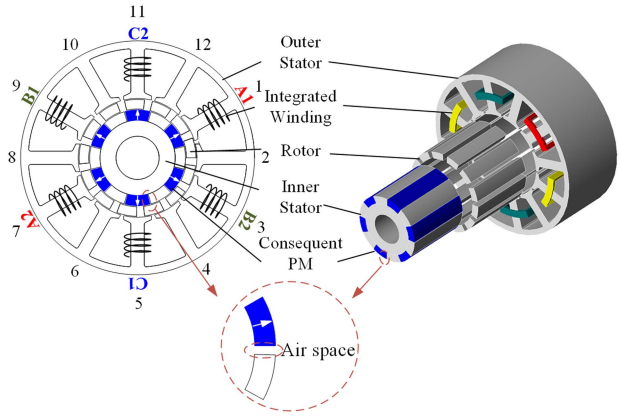

Fig. 1. Structure of the proposed DS-HEM.

To obtain the optimal control performance of an HEM, this article proposes an MTPA cooperative control strategy of a double stator dc-bias HEM (DS-HEM) with dc-bias current, establishing a mathematical model of DS-HEM with dc-bias current, and considers the inductance nonlinearity. The main contributions of this article are as follows.

1) The proposed double stator structure can eliminate the space conflicts, aiming to further improve the torque density, and the proposed hybrid excitation with dc bias can improve the flux regulation capability and efficiency.
2) This article establishes the mathematical model of the DS-HEM considering the inductance nonlinearity and the quadratic polynomial model of inductance is established based on the voltage under different currents and speeds.
3) An MTPA cooperative control strategy of the DS-HEM from two dimensions of the armature current and dc-bias current is proposed. The proposed strategy can achieve high torque density and low copper loss. Comparative studies and experimental results demonstrate the effectiveness of the proposed method.

This article is organized as follows. In Section II, the topology and basic principle of DS-HEM are presented. In Section III, the principle and procedure of the proposed MTPA cooperative control strategy are introduced, and the inductance nonlinear model is established. Section IV, the experimental tests are carried out to validate the proposed method. Finally, Section V concludes this article.

II. Topology and Mathematical Model

A. Machine Structure and Drive System

Fig. 1 shows the structure of the proposed DS-HEM, which mainly consists of the inner stator, rotor, and outer stator. The double stator separates the armature winding and stator-PM on different stators, thus eliminating the space conflicts. Consequent-pole PMs are inset on the inner stator part, which is radically magnetized. Iron pieces form the sandwich rotor, which

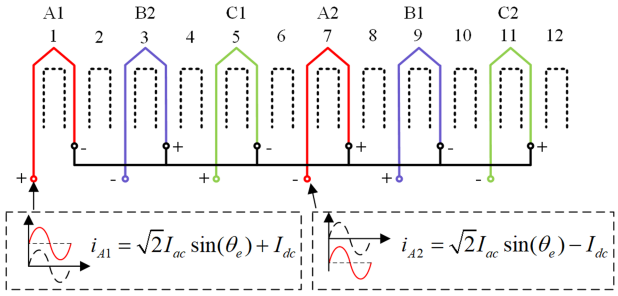

Fig. 2. Winding connection of integrated winding.

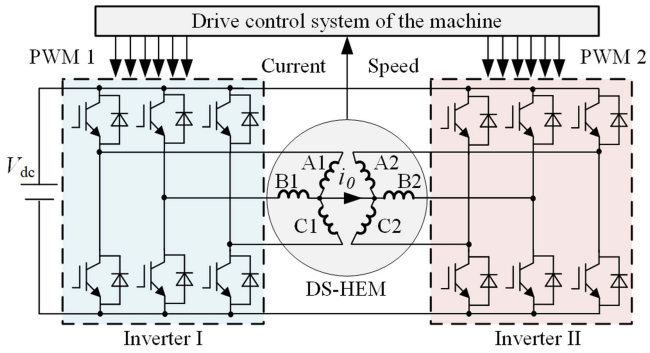

Fig. 3. Dual three-phase drive circuit of the DS-HEM.

is used as the flux modulation poles of dc-bias current and PMs. The armature winding is a dual three-phase configuration that has the windings A1B1C1 and A2B2C2, and dc-bias current is integrated into the armature winding.

The winding connection of the DS-HEM is shown in Fig. 2, which adopts dual three-phase integrated windings. The combined sinusoidal current and dc, called dc-biased sinusoidal current, is injected into the windings to drive the machine. The current of each phase in the dual three-phase windings with dc bias can be expressed as

$$\begin{cases} I_{A1} = \sqrt{2} i_{\text{ac}} \sin(\theta_e) + I_{\text{dc}} \\ I_{B1} = \sqrt{2} i_{\text{ac}} \sin(\theta_e - 2\pi/3) + I_{\text{dc}} \\ I_{C1} = \sqrt{2} i_{\text{ac}} \sin(\theta_e + 2\pi/3) + I_{\text{dc}} \\ I_{A2} = \sqrt{2} i_{\text{ac}} \sin(\theta_e) - I_{\text{dc}} \\ I_{B2} = \sqrt{2} i_{\text{ac}} \sin(\theta_e - 2\pi/3) - I_{\text{dc}} \\ I_{C2} = \sqrt{2} i_{\text{ac}} \sin(\theta_e + 2\pi/3) - I_{\text{dc}} \end{cases} \tag{1}$$

where i_{ac} is the root-mean-square (RMS) value of alternating current, θ_e is the electrical angle of the machine, which can be expressed as $\theta_e = N_r \omega_r t$, N_r is the number of rotor poles, ω_r is the mechanical speed of the machine, and I_{dc} is the value of dc-bias current.

The dual three-phase drive circuit of the proposed machine is shown in Fig. 3. Two three-phase inverters are connected to two sets of armature winding, respectively. The armature current and dc-bias current are controlled by a cooperative control strategy. The ac component of the current on the two sets of windings is the same, and the dc component is equal and opposite.

B. Mathematical Model of DS-HEM

In the natural coordinate system, the voltage equation of the DS-HEM is given by

$$\mathbf{u_s} = R_s \mathbf{i_s} + \frac{d\boldsymbol{\psi}_{\mathbf{m}}}{dt} + \frac{d\mathbf{L_s i_s}}{dt} \tag{2}$$

where $\mathbf{u_s} = [u_{A1}, u_{B1}, u_{C1}, u_{A2}, u_{B2}, u_{C2}]^T$ represents the voltage of stator windings, $\mathbf{i_s} = [i_{A1}, i_{B1}, i_{C1}, i_{A2}, i_{B2}, i_{C2}]^T$ represents the current of stator windings, R_s is the resistance of individual windings, ψ_m is the flux linkage of a permanent magnet, and $\mathbf{L_s}$ is the inductance matrix in the dual three-phase configuration, which changes with the electrical angle of the machine and can be expressed as [24], [30]

$$\mathbf{L_s}(\theta_e) = \begin{bmatrix} \mathbf{L}_{(3\times3)}(\theta_e) & \mathbf{M}_{(3\times3)}(\theta_e) \\ -\mathbf{M}_{(3\times3)}(\theta_e) & -\mathbf{L}_{(3\times3)}(\theta_e) \end{bmatrix} \tag{3}$$

where $\mathbf{L}_{(3\times3)}$ represents the inductance between the same windings, and $\mathbf{M}_{(3\times3)}$ is the inductance between the different windings, and respectively can be expressed as [24], [30]

$$\mathbf{L}_{(3\times3)}(\theta_e) = \begin{bmatrix} \mathbf{L}(\theta_e) & \mathbf{M_1}(\theta_e + \frac{2}{3}\pi) & \mathbf{M_1}(\theta_e - \frac{2}{3}\pi) \\ \mathbf{M_1}(\theta_e + \frac{2}{3}\pi) & \mathbf{L}(\theta_e - \frac{2}{3}\pi) & \mathbf{M_1}(\theta_e) \\ \mathbf{M_1}(\theta_e - \frac{2}{3}\pi) & \mathbf{M_1}(\theta_e) & \mathbf{L}(\theta_e + \frac{2}{3}\pi) \end{bmatrix} \tag{4}$$

$$\mathbf{M}_{(3\times3)}(\theta_e) = \begin{bmatrix} \mathbf{M_2}(\theta_e) & \mathbf{M_3}(\theta_e - \frac{2}{3}\pi) & \mathbf{M_3}(\theta_e + \frac{2}{3}\pi) \\ \mathbf{M_3}(\theta_e) & \mathbf{M_2}(\theta_e - \frac{2}{3}\pi) & \mathbf{M_3}(\theta_e + \frac{2}{3}\pi) \\ \mathbf{M_3}(\theta_e) & \mathbf{M_3}(\theta_e - \frac{2}{3}\pi) & \mathbf{M_2}(\theta_e + \frac{2}{3}\pi) \end{bmatrix} \tag{5}$$

where the self-inductive component and mutual inductance component in (4) and (5) are given by [24], [30]

$$\begin{cases} \mathbf{L}(\theta_e) = L_0 + \sum_{i=1,3,5\ldots} L_i \cos(i\theta) - \sum_{j=2,4,6\ldots} L_j \cos(j\theta) \\ \mathbf{M_1}(\theta_e) = M_{01} + \sum_{i=1,3,5\ldots} M_{i1} \cos(i\theta) \\ \qquad\qquad - \sum_{j=2,4,6\ldots} M_{j1} \cos(j\theta) \\ \mathbf{M_2}(\theta_e) = M_{02} + \sum_{i=1,3,5\ldots} M_{i2} \cos(i\theta) \\ \qquad\qquad - \sum_{j=2,4,6\ldots} M_{j2} \cos(j\theta) \\ \mathbf{M_3}(\theta_e) = M_{03} + \sum_{i=1,3,5\ldots} M_{i3} \cos(i\theta) \\ \qquad\qquad - \sum_{j=2,4,6\ldots} M_{j3} \cos(j\theta) \end{cases} \tag{6}$$

where L_i $(i = 1, 3, 5\ldots,)$ and L_j $(j = 2, 4, 6\ldots,)$ are the *i*th and *j*th harmonic components of self-inductance, respectively, M_{i1} and M_{j1} are the *i*th and *j*th mutual inductances between different phases in the same set of windings, respectively, M_{i2} and M_{j2} represent the *i*th and *j*th mutual inductances between the same phase in two sets of different windings, respectively, and M_{i3} and M_{j3} indicate the *i*th and *j*th mutual inductances between different phases in two sets of different windings, respectively.

In the different harmonic components of the inductance, the fundamental component is close to the constant component, and the interaction of the fundamental component and the constant component of inductance generates the average torque [31].

Thus, in the subsequent analysis, only the constant and fundamental components of inductance are considered to simplify the mathematical model of the machine.

Because there are nonlinear components in the mathematical model of the machine in the natural coordinate system, coordinate transformation is adopted, that is, the transformation of the coordinate system synchronized with the rotor speed. To obtain the voltage equation in the *dq*0-axis, the transformation matrix is used as

$$\mathbf{T}_{ABC/dq0}(\theta_e)=\begin{bmatrix}\mathbf{T}_\theta(\theta_e) & \mathbf{0}_{(3\times3)}\\ \mathbf{0}_{(3\times3)} & \mathbf{T}_\theta(\theta_e)\end{bmatrix} \tag{7}$$

where

$$\mathbf{T}_\theta(\theta_e)=\frac{2}{3}\begin{bmatrix}\cos(\theta_e) & \cos(\theta_e-\frac{2}{3}\pi) & \cos(\theta_e+\frac{2}{3}\pi)\\ -\sin(\theta_e) & -\sin(\theta_e-\frac{2}{3}\pi) & -\sin(\theta_e+\frac{2}{3}\pi)\\ \frac{1}{2} & \frac{1}{2} & \frac{1}{2}\end{bmatrix} \tag{8}$$

and $\mathbf{0_{(3\times3)}}$ is a 3×3 dimensional zero matrix, thus the voltage equation of the DS-HEM in the *dq*0-axis can be expressed as [24]

$$\mathbf{u_{dq0}}=R_s\mathbf{i_{dq0}}+\mathbf{L_{dq0}}\frac{d}{dt}(\mathbf{i_{dq0}})+\omega_e\mathbf{L'_{dq0}}\mathbf{i_{dq0}}+\omega_e\boldsymbol{\psi}_\mathbf{m} \tag{9}$$

where $\mathbf{u_{dq0}}=[u_{d1},u_{q1},u_{01},u_{d2},u_{q2},u_{02}]^T$ represents the voltage under the *dq*0-axis and $\mathbf{I_{dq0}}=[i_{d1},i_{q1},i_{01},i_{d2},i_{q2},i_{02}]^T$ represents the current under the *dq*0-axis. It should be mentioned that, after a coordinate transformation, the values of 0-axis current i_0 and dc-bias current $I_{\rm dc}$ are identical. $\mathbf{L_{dq0}}$ is the inductance matrix under the *dq*0-axis, which can be expressed as

$$\mathbf{L_{dq0}}=T_{ABC/dq0}(\theta_e)\mathbf{L_s}(\theta_e){T^{-1}}_{ABC/dq0}(\theta_e) \tag{10}$$

when the machine is working steadily, $d(\mathbf{i_{dq0}})/dt=0$, thus $\mathbf{L_{dq0}}$ is negligible. $\mathbf{L'_{dq0}}$ is the coupling inductance matrix, which is given by [30]

$$\mathbf{L'_{dq0}}=\begin{bmatrix}\mathbf{L'}_{dq0(3\times3)} & \mathbf{M'}_{dq0(3\times3)}\\ \mathbf{M'}_{dq0(3\times3)} & \mathbf{L'}_{dq0(3\times3)}\end{bmatrix} \tag{11}$$

$$\mathbf{L'}_{dq0(3\times3)}=\begin{bmatrix}0 & -(L_0+M_{01}) & 0\\ L_0+M_{01} & 0 & L_1-M_{11}\\ 0 & 0 & 0\end{bmatrix} \tag{12}$$

$$\mathbf{M'}_{dq0(3\times3)}=\begin{bmatrix}0 & -(M_{02}-M_{03}) & 0\\ M_{02}-M_{03} & 0 & M_{12}+M_{12}\\ 0 & 0 & 0\end{bmatrix} \tag{13}$$

where L_0, L_1, M_{01}, M_{11}, M_{02}, M_{12}, M_{03}, and M_{13}, are explained in (6). For the proposed DS-HEM, the ac in the two windings groups are the same, and the dc has an opposite direction, therefore, define $i_d=i_{d1}=i_{d2}$, $i_q=i_{q1}=i_{q2}$, $i_0=i_{01}=-i_{02}$, $L_s=L_1+M_1+M_2-M_3$, and $L_m=L_1-M_{11}+M_{12}+M_{13}$, and the voltage equation in (9) can be concretely expressed as

$$\begin{cases}u_{d1}=R_si_d-\omega_eL_si_q\\ u_{q1}=R_si_q+\omega_eL_si_d+\omega_eL_mi_0+\omega_e\psi_m\\ u_{01}=R_si_0\\ u_{d2}=R_si_d-\omega_eL_si_q\\ u_{q2}=R_si_q+\omega_eL_si_d+\omega_eL_mi_0+\omega_e\psi_m\\ u_{02}=-R_si_0\end{cases}. \tag{14}$$

Moreover, the flux linkage equation of the DS-HEM can be expressed as

$$\begin{cases}\psi_d=2(L_si_d+L_mi_0+\psi_m)\\ \psi_q=2L_si_q\end{cases}. \tag{15}$$

The average torque is produced by the sum of two winding groups, and it can be expressed as

$$T_e=\frac{3}{2}p(i_q\psi_d-i_d\psi_q)=3p(L_mi_0i_q+\psi_mi_q). \tag{16}$$

Hence, it indicates that the output torque can be generated by the interaction of armature winding and two excitation sources including dc-bias current and consequent-pole PMs.

TABLE I
PARAMETERS OF THE PROPOSED DS-HEM

Parameter	Unit	Value
PM grade	/	N38SH
PM remanence	T	1.2
PM coercive force	kA/m	965
Silicon steel Grade	/	35JN270
PM height	mm	6
PM angle	°	30.1
Stator iron piece angle	°	27.4
Rotor iron piece angle	°	19.8
Outer stator yoke width	mm	4
Outer stator tooth width	mm	7
Outer stator tooth–tang width	mm	14.5
Outer stator tooth–tang depth	mm	1.4
Air-gap length	mm	0.5
Stack length	mm	50
Turn number of coils	/	74

III. CONTROL STRATEGY

In this section, a 12/13 DS-HEM finite element analysis (FEA) model is developed. Based on this model, an MTPA cooperative control strategy considering inductance nonlinearity is proposed. Table I shows the parameters of the proposed DS-HEM.

A. Effect of DC-Bias Current on Machine Performance

For DS-HEM, there is an additional dc-bias current in armature windings, which can be positive to enhance the air-gap flux density and improve the torque or negative to weaken the air-gap flux density and broaden the speed range. Hence, the injection of dc-bias current can not only increase the torque but also flexibly adjust the air-gap flux density. To illustrate the importance of the cooperative control of armature current and excitation current,

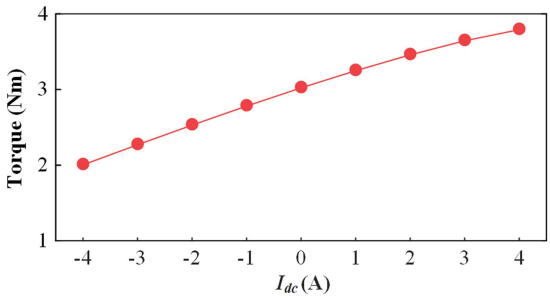

Fig. 4. Torque versus $I_{\rm dc}$ ($i_{\rm ac} = 8$ A).

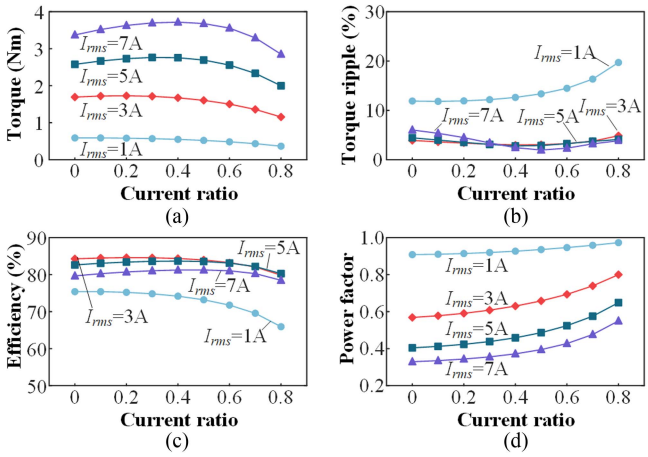

Fig. 5. Influence of $I_{\rm rms}$ with current ratio k on DS-HEM. (a) Average torque. (b) Torque ripple. (c) Efficiency. (d) Power factor.

it is necessary to first investigate the effect of dc-bias current on the machine performance.

Fig. 4 shows the variations of $I_{\rm dc}$ on the average torque of DS-HEM. It shows that with the variation of $I_{\rm dc}$, the change of the torque of DS-HEM is obvious, which is because the PM flux and dc flux in the proposed DS-HEM are parallel, so they won't interfere with each other. Consequently, it demonstrates that changing $I_{\rm dc}$ can adjust the magnetic field of the machine.

For HEMs, the ratio of injected dc is vital because it affects both the field excitation and armature excitation with the constant total current. The RMS value of the total current can be defined as

$$I_{\rm rms} = \sqrt{i_{\rm ac}^2 + I_{\rm dc}^2}. \tag{17}$$

Then, define the current ratio of k

$$k = \frac{I_{\rm dc}}{I_{\rm rms}}. \tag{18}$$

The effect of the change of the current ratio k with different $I_{\rm rms}$ on the performance of DS-HEM is shown in Fig. 5. It can be found that both average torque and efficiency of DS-HEM show a trend of initially rising and then falling with the increase of k, while the change of torque ripple is the opposite, which means the maximal average torque, the minimal torque ripple, and highest efficiency can be reached. It should be mentioned that, to calculate the efficiency, the copper losses, iron losses, and PM losses of the DS-HEM are considered. Moreover, the injection of dc-bias current is beneficial for the power factor. The optimal current ratio of DS-HEM is between 0.4 and 0.6 considering a tradeoff among average torque, torque ripple, efficiency, and power factor. The copper loss can be well controlled when the optimal torque performance is achieved. Therefore, it demonstrates that the dc-bias current has a significant impact on machine performance, the armature current and dc-bias current should be cooperatively controlled, to achieve optimal performance.

B. Proposed MTPA Cooperative Control Strategy

The traditional MTPA method is based on $i_d = 0$ control, the current ratio of i_q and i_0 is fixed, which is $i_q = \sqrt{2} i_0$. It has the advantage of being simple to implement. However, the traditional i_0-fixed method does not use *0*-axis current as an additional degree of freedom. Consequently, to obtain the best performance of the machine, the proposed MTPA cooperative control strategy from two dimensions of armature and excitation currents is introduced.

The total copper loss of the DS-HEM can be expressed as

$$P_c = 6R_s\left(\frac{i_q^2}{2} + i_0^2\right) \tag{19}$$

where R_s is the resistance of a set of windings. The optimal combination of i_q and i_0 can be obtained according to a Lagrange extremum function, which is defined by

$$F(i_0, i_q, \lambda) = 3p(L_m i_0 i_q + \psi_m i_q) + \lambda\left[P_c - 6R_s\left(\frac{i_q^2}{2} + i_0^2\right)\right] \tag{20}$$

where λ is the Lagrange multiplier. The partial derivative of the Lagrange extremum equation concerning i_q, i_0, and λ is acquired by

$$\begin{cases} \frac{\partial F(i_0,i_q,\lambda)}{\partial i_0} = 3pL_m i_q - 12\lambda R_s i_0 = 0 \\ \frac{\partial F(i_0,i_q,\lambda)}{\partial i_q} = 3p(L_m i_0 + \psi_m) - 6\lambda R_s i_q = 0 \\ \frac{\partial F(i_0,i_q,\lambda)}{\partial \lambda} = P_c - 6R_s(\frac{i_q^2}{2} + i_0^2) = 0 \end{cases}. \tag{21}$$

Then the solution can be obtained as

$$\begin{cases} i_q = \left(\frac{4L_m^2 P_c - 6R_s\psi_m^2 + \sqrt{3}R_s\psi_m\sqrt{\frac{16P_cL_m^2 + 12R_s\psi_m^2}{R_s}}}{24L_m^2 R_s}\right)^{\frac{1}{2}} \\ i_0 = \frac{-2\psi_m + \sqrt{\frac{16P_cL_m^2 + 12R_s\psi_m^2}{R_s}}}{8L_m} \end{cases}. \tag{22}$$

Since the copper loss is proportional to $I_{\rm rms}$, for a given $I_{\rm rms}$, we can use (22) to find the current distribution at the maximum torque.

Nonetheless, R_s, ψ_m, and L_m are the parameters that need to be obtained in advance. The resistance and PM flux linkage are relatively fixed, but L_m is a nonlinear parameter with i_d, i_q, and i_0. Thus, to improve the accuracy of the MTPA cooperative control strategy, it is vital to establish the nonlinear inductance model.

C. Inductance Nonlinearity Modeling

The inductances of the machine are nonlinear with the current because of magnetic saturation. To make the inductance model suitable for a wide range of operating conditions and improve the accuracy of the control strategy, this article considers inductance as a quadratic polynomial model with respect to i_d, i_q, and i_0. Nonetheless, as the $i_d = 0$ control strategy is applied in the proposed strategy, inductances depend on i_q and i_0 only. Thus, the inductances in the *dq*0-axis can be denoted as

$$\begin{cases} L_s(I_q, I_0) = \alpha_0 + \alpha_1 I_q + \alpha_2 I_0 + \alpha_3 I_q^2 + \alpha_4 I_0^2 + \alpha_5 I_q I_0 \\ L_m(I_q, I_0) = \beta_0 + \beta_1 I_q + \beta_2 I_0 + \beta_3 I_q^2 + \beta_4 I_0^2 + \beta_5 I_q I_0 \end{cases} \tag{23}$$

where $\alpha_0, \ldots, \alpha_5$ and $\beta_0, \ldots, \beta_5$ are the coefficients of the quadratic model. Hence, the voltage equation considering $i_d = 0$ control strategy and inductance nonlinearity can be expressed as

$$\begin{cases} U_{d1} = -\omega_e L_s(I_q, I_0) I_q \\ U_{q1} = R_s I_q + \omega_e L_m(I_q, I_0) I_0 + \omega_e \psi_m \\ U_{01} = R_s I_0 \\ U_{d2} = -\omega_e L_s(I_q, I_0) I_q \\ U_{q2} = R_s I_q + \omega_e L_m(I_q, I_0) I_0 + \omega_e \psi_m \\ U_{02} = -R_s I_0 \end{cases}. \tag{24}$$

As the equation of two sets of windings is similar, only one set of three-phase windings of the machine is considered. To facilitate subsequent calculation, the voltage equation in the $DQ0_1$ frame in (22) can be rewritten as

$$\begin{cases} U_{d01} = U_{d1} + U_{01} = R_s I_0 - \omega_e L_s(I_q, I_0) I_q \\ U_{q1} = R_s I_q + \omega_e L_m(I_q, I_0) I_0 + \omega_e \psi_m \end{cases}. \tag{25}$$

Then, four variables m_1, m_2, n_1, and n_2 which are independent of speed are defined to improve the efficiency of calculation, these four variables can be calculated first, and then the other parameters. The four variables can be expressed as

$$\begin{cases} m_1 = R_s I_0 \\ m_2 = R_s I_q \\ n_1 = (\alpha_0 + \alpha_1 I_q + \alpha_2 I_0 + \alpha_3 I_q^2 + \alpha_4 I_0^2 \\ \qquad +\alpha_5 I_q I_0) I_q \\ n_2 = (\beta_0 + \beta_1 I_q + \beta_2 I_0 + \beta_3 I_q^2 + \beta_4 I_0^2 \\ \qquad +\beta_5 I_q I_0) I_0 + \psi_m \end{cases}. \tag{26}$$

The voltage equation in (25) can be updated by applying (26) as

$$\begin{cases} U_{d01} = m_1 - \omega_e n_1 \\ U_{q1} = m_2 + \omega_e n_2 \end{cases}. \tag{27}$$

It should be noted that m_1, m_2, n_1, and n_2 vary with the current in the *DQ*0 frame, but are independent of the speed of the machine. Given that I_q, I_0, m_1, m_2, n_1, n_2 are constant, for a certain (I_q, I_0), the voltages are collected at *N* different speed (term as $\omega_{e1}, \ldots, \omega_{eN}$), then these voltages should satisfy as

$$\begin{cases} U_{d01,n} = m_1 - \omega_{en} n_1 \\ U_{q1,n}, n = m_2 + \omega_{en} n_2 \end{cases}, n = 1, \ldots, N \tag{28}$$

where $U_{d01,n}$ and $U_{q1,n}$ are acquired at the speed of ω_{en}, and thus m_1, m_2, n_1, and n_2 can be acquired by using the least squares method as expressed in (29). It can be known that at least two different speed conditions should be measured, and the accuracy of calculation can be improved by using data at more different speed.

$$M_1 = (\Phi_1^T \Phi_1)^{-1} \Phi_1^T N_1 \tag{29}$$

where

$$M_1 = \begin{bmatrix} m_1 \\ m_2 \\ n_1 \\ n_2 \end{bmatrix}, \Phi_1 = \begin{bmatrix} 1 & 0 & -\omega_1 & 0 \\ 0 & 1 & 0 & \omega_1 \\ & & \vdots & \\ 1 & 0 & -\omega_N & 0 \\ 0 & 1 & 0 & \omega_N \end{bmatrix}, N_1 = \begin{bmatrix} U_{d01,1} \\ U_{q1,1} \\ \vdots \\ U_{d01,N} \\ U_{q1,N} \end{bmatrix}. \tag{30}$$

For a particular set of (I_q, I_0), the corresponding (m_1, m_2, n_1, n_2) can be obtained. By using (m_1, m_2, n_1, n_2) from different (I_q, I_0), the coefficients of inductance can be acquired from the following steps.

For a certain pair $\{n_{1,k}, k = 1, \ldots, K\}$, $n_{1,k}$ can be denoted as

$$\begin{aligned} n_{1,k} = (&\alpha_0 + \alpha_1 I_{q,k} + \alpha_2 I_{0,k} + \alpha_3 I_{q,k}^2 \\ &+ \alpha_4 I_{0,k}^2 + \alpha_5 I_{q,k} I_{0,k}) I_{q,k}. \end{aligned} \tag{31}$$

Hence, $\alpha_0, \ldots, \alpha_5$ can be estimated from

$$M_2 = (\Phi_2^T \Phi_2)^{-1} \Phi_2^T N_2 \tag{32}$$

where

$$M_2 = \begin{bmatrix} \alpha_0 & \alpha_1 & \ldots & \alpha_5 \end{bmatrix}^T \tag{33}$$

$$N_2 = \begin{bmatrix} n_{1,1} & n_{1,2} & \cdots & n_{1,K} \end{bmatrix}^T \tag{34}$$

$$\Phi_2 = \begin{bmatrix} I_{q,1} & I_{q,1}^2 & I_{0,1} I_{q,1} & I_{q,1}^3 & I_{0,1}^2 I_{q,1} & I_{q,1}^2 I_{0,1} \\ & & & \vdots & & \\ I_{q,K} & I_{q,K}^2 & I_{0,K} I_{q,K} & I_{q,K}^3 & I_{0,K}^2 I_{q,K} & I_{q,K}^2 I_{0,K} \end{bmatrix}. \tag{35}$$

To avoid rank deficiency, *K* should be more than 6, and more measurements from multiple conditions can ensure the accuracy of the calculation.

For a certain pair $\{n_{2,k}, k = 1, \ldots, K\}$, $n_{2,k}$ can be expressed as

$$\begin{aligned} n_{2,k} = (&\beta_0 + \beta_1 I_{q,k} + \beta_2 I_{0,k} + \beta_3 I_{q,k}^2 \\ &+ \beta_4 I_{0,k}^2 + \beta_5 I_{q,k} I_{0,k}) I_{0,k} + \psi_m. \end{aligned} \tag{36}$$

It should be noted that the result of ψ_m will affect the estimation result of L_m, so it is considerable to obtain ψ_m first to improve the accuracy of the inductance, therefore, $\beta_0, \ldots, \beta_5$ can be estimated from

$$M_3 = (\Phi_3^T \Phi_3)^{-1} \Phi_3^T N_3 \tag{37}$$

where

$$M_3 = \begin{bmatrix} \beta_0 & \beta_1 & \ldots & \beta_5 \end{bmatrix}^T \tag{38}$$

$$N_3 = \begin{bmatrix} n_{2,1} & n_{2,2} & \cdots & n_{2,K} \end{bmatrix}^T - \psi_m \tag{39}$$

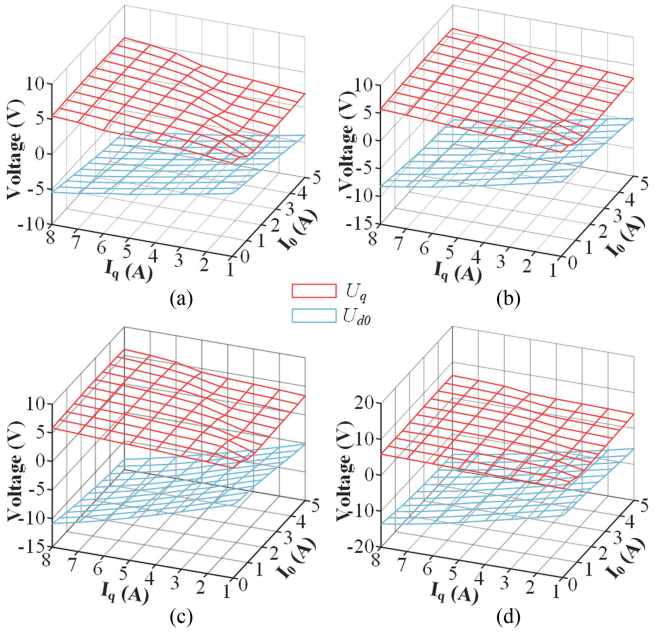

Fig. 6. Measured voltages under various current conditions at different speeds. (a) 100 r/min. (b) 150 r/min. (c) 200 r/min. (d) 250 r/min.

TABLE II
VALUES OF THE COEFFICIENTS

Paramete	Value	Paramete	Value
α_0	4.6×10^{-3}	β_0	7.6×10^{-3}
α_1	8.8×10^{-4}	β_1	-7.5×10^{-5}
α_2	-4.5×10^{-4}	β_2	-5.6×10^{-4}
α_3	4.1×10^{-5}	β_3	2.2×10^{-5}
α_4	2.8×10^{-6}	β_4	3.0×10^{-5}
α_5	7.9×10^{-5}	β_5	2.3×10^{-6}

$$\Phi_3 = \begin{bmatrix} I_{0,1} & I_{0,1}I_{q,1} & I_{0,1}^2 & I_{q,1}^2 I_{0,1} & I_{0,1}^3 & I_{0,1}^2 I_{q,1} \\ & & & \vdots & & \\ I_{0,K} & I_{0,K}I_{q,K} & I_{0,K}^2 & I_{q,K}^2 I_{0,K} & I_{0,K}^3 & I_{0,K}^2 I_{q,K} \end{bmatrix}. \tag{40}$$

Also, K should be no less than 6 to estimate these coefficients. After $\alpha_0, \ldots, \alpha_5$ and $\beta_0, \ldots, \beta_5$ are estimated, L_m and L_s can be calculated from (23).

To perform the proposed nonlinear inductance model, the reference current for I_d is set to 0, for I_q the reference current is set to 1, 2, 3, …, 8 A; and that for I_0 is set to 0, 0.5, 1, …, 5 A; the speed of the machine is set to 100, 150, 200, 250 r/min. Under these conditions, the voltages in the $DQ0_1$ frame are collected and shown in Fig. 6. With these measurements and the procedures mentioned above, the nonlinear inductance model is built. The coefficients of the quadratic model are listed in Table II. The calculation results for inductances L_m and L_s are shown in Fig. 7. It shows that, with the increase of both i_q and i_0, L_m decreases, while for L_s, the change of i_0 has little effect on it. This is because L_m is the inductance generated by the coupling of ac and dc, it is related to both i_q and i_0, and L_s is similar to the synchronous inductance related to the armature current, so i_0 has little influence on it.

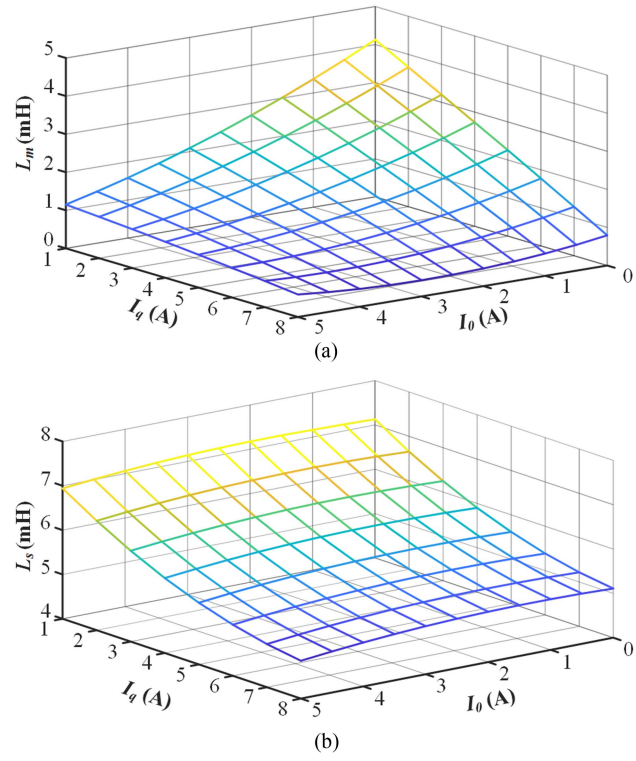

Fig. 7. Inductance estimation results. (a) L_{m}. (b) L_{s}.

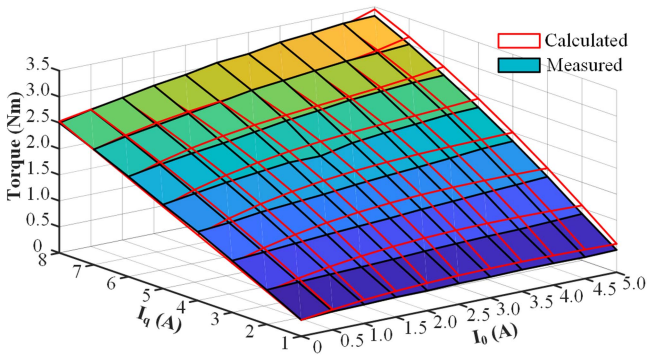

Fig. 8. Torque measured at 150 r/min against calculation.

After acquiring the inductance, the accuracy of the inductance can be verified by using (16). The measured resistance of the individual windings is 0.38 Ω, and the flux linkage of the permanent magnet is 0.0081 Wb. The torque of different currents at 150 r/min is compared with the calculated torque, as shown in Fig. 8. It demonstrates that the calculated results are in good agreement with the experimental results, which illustrates the high accuracy of the proposed nonlinear inductance model.

IV. EXPERIMENTAL RESULTS

To verify the effectiveness of the proposed method, a prototype of the proposed DS-HEM is manufactured, as shown in Fig. 9. The experimental platform is shown in Fig. 10. The drive control system mainly includes two 5.0 kW three-phase

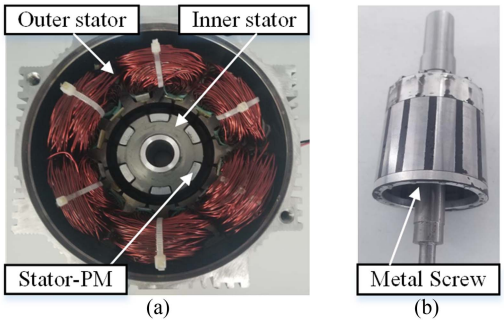

Fig. 9. Prototype. (a) Outer stator and inner stator. (b) Rotor.

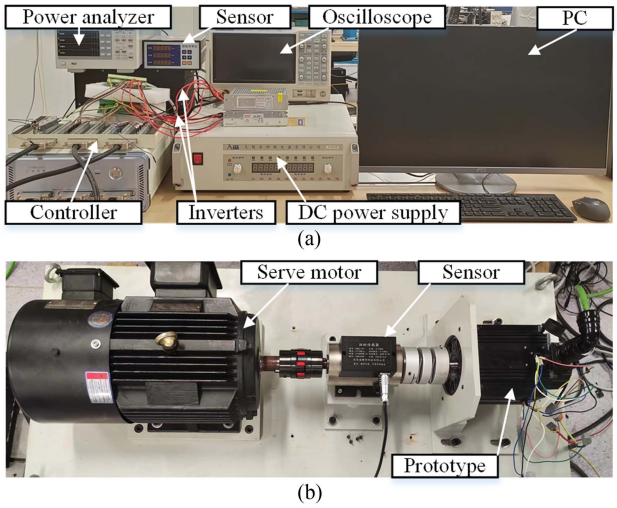

Fig. 10. Test platform. (a) Drive devices. (b) Test bench.

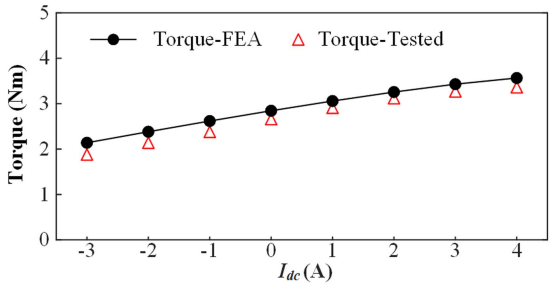

Fig. 11. Torque against $I_{\rm dc}$ ($i_{\rm ac} = 8$ A).

full-bridge inverters, a 6.0 kW dc power supply, and an MT 1050 controller for controlling the proposed machine. The test bench mainly consists of a prototype, an 11.0 kW PM servo motor for producing load torque, incremental encoders with 2500 pulses/revolution, and a torque sensor.

A. Experimental Verification

To verify the performance of the prototype, the variations of average torque versus different $I_{\rm dc}$ are simulated by FEA and measured in the experiment, as shown in Fig. 11. It indicates that with the increasing of $I_{\rm dc}$ from -3 to 4 A, the average torque

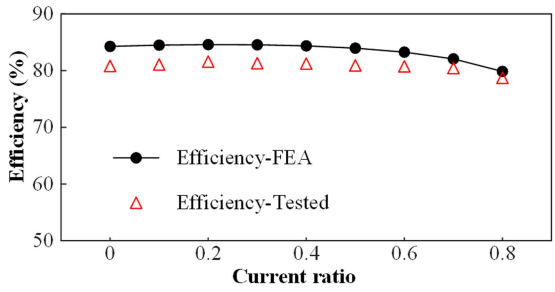

Fig. 12. Efficiency under different current ratios ($I_{\rm rms} = 3$ A).

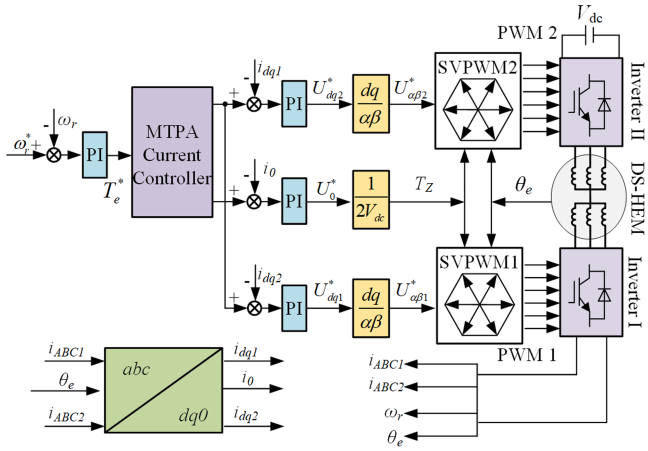

Fig. 13. Proposed control method block diagram using dual three-phase drive circuit for DS-HEM.

varies from 1.86 to 3.18 N·m, and the experimental average torque has a good agreement with that of FEA. In addition, it shows the flux-enhancing and flux-weakening operation of the proposed machine can be achieved by injecting the positive or negative dc-bias current.

Fig. 12 shows the efficiency comparison between the simulation and experiments at different current ratios when $I_{\rm rms} = 3$ A and the rotation speed is 1000 r/min. It shows the experimental efficiency is relatively consistent with the simulated efficiency, which has a difference of about 3%–4%, and the efficiency errors are mainly due to the end effect and manufacturing deviation.

B. Implement of Proposed MTPA Cooperative Control Strategy

The overall control system with dual three-phase inverters of the proposed DS-HEM is shown in Fig. 13. The 0-axis reference current satisfies $i_0 = i_{01} = -i_{02}$ and i_0 is acquired from i_{ABC1} through Park's transformation. To generate a dc-bias current, opposite zero sequence voltage is added into the dual three-phase windings, which can be regulated by the closed-loop current controller in the 0-axis. When giving a value of $I_{\rm rms}$, the optimal values of i_0 and i_q are calculated from the proposed MTPA cooperative controller.

Fig. 14 presents the average torque measured and calculated under different $I_{\rm rms}$. It can be found that there is a slight

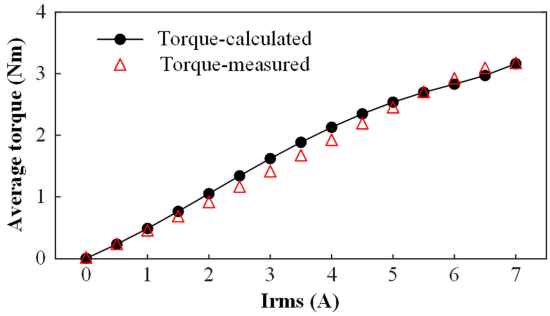

Fig. 14. Average torque measured and calculated under different I_{rms}.

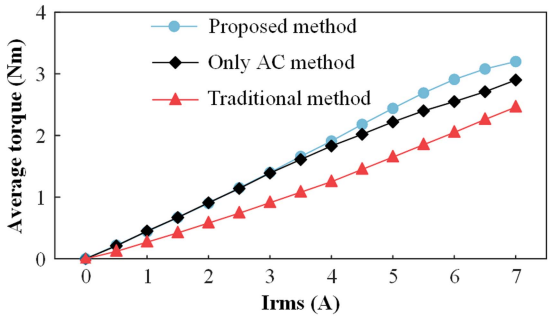

Fig. 15. Average torque measured using different methods under different I_{rms}.

difference of around 0.2 N·m between the measurement and calculation when I_{rms} increases from 0 to 7 A. It demonstrates the accuracy of the proposed model, and the difference is because of the deviation between the calculated inductance and the actual inductance.

To verify the superiority of the proposed MTPA cooperative control strategy, comparative studies are conducted. Two existing control strategies, the only ac method and the traditional fixed current ratio method [18] are carried out. The only ac method does not inject the dc-bias current, and the traditional method fixes the current ratio, which is $i_q = 1.414 i_0$. Fig. 15 shows the average torques with three methods under different I_{rms}. When I_{rms} is less than 3A, the proportion of i_0 is relatively small in the proposed method, the machine is mainly operated by i_q. Moreover, the effect of i_0 on the machine performance is relatively small when I_{rms} is small, thus, the torque difference between the only ac method and the proposed method is small when I_{rms} is less than 3A. With the increase of I_{rms}, the torque difference between the two methods gradually becomes large. Besides, the difference in the average torque between the proposed method and the traditional method is larger. When I_{rms} is 4 and 8 A, the average torque of the proposed method is 0.66 N·m and 0.72 N·m larger than that of the traditional method, respectively. Hence, it verifies that the proposed control method considering i_0 as an extra dimension can achieve optimal performance.

Fig. 16 shows the load control process of the proposed method at 500 r/min when I_{rms} changes from 5 to 6 A. The output torque increases from 2.44 to 2.91 N·m steadily. Thus, the proposed machine can achieve flexible variable load control.

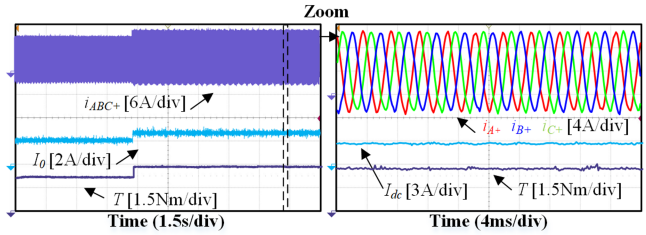

Fig. 16. Experimental results using the proposed method.

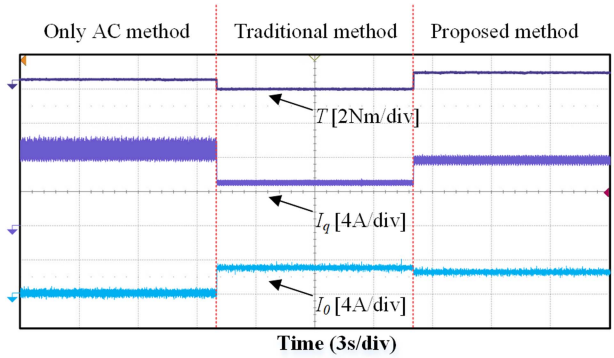

Fig. 17. Experimental results of three methods under the same I_{rms}.

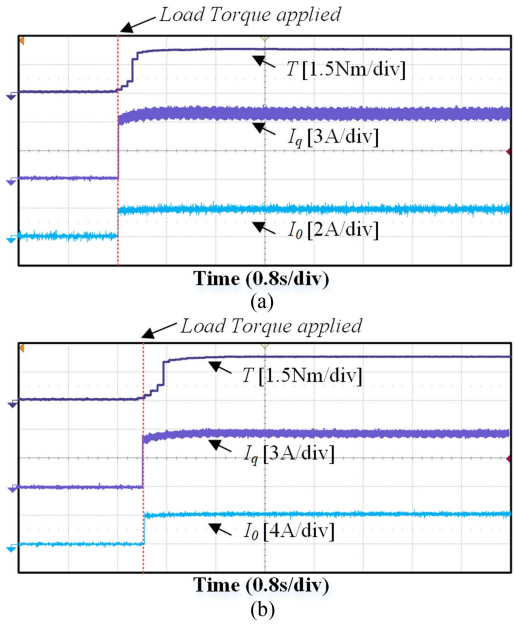

Fig. 18. Transient torque response at 500 r/min. (a) Proposed method. (b) Conventional method.

Fig. 17 shows the current distribution and torque comparison results of three methods under the same I_{rms}. When $I_{\text{rms}} = 6$ A, the output torque of the proposed method is 2.91 N·m, whereas the output torques of the traditional method and the only ac method are 2.05 N·m and 2.55 N·m, respectively. Compared with the only ac method, the proposed method injects the 0-axis current to regulate the air-gap flux density and enhance the torque. Meanwhile, different from the traditional method, the proposed

method considers i_0 as an additional degree of freedom, and can flexibly change i_0 to achieve the optimal performance. Hence, the proposed MTPA cooperative control strategy can achieve higher output torque under the same currents.

The transient performance in the constant torque region, when the load torque is varied from 0 to 2.50 N·m, is investigated. The comparison of the transient responses of the output torque, i_0 and i_q between the proposed method and conventional methods are shown in Fig. 18. When applying a 2.50 N·m load torque, $I_{\rm rms}$ of the conventional method is about 7 A, whereas $I_{\rm rms}$ of the proposed method is reduced to 5 A. Therefore, the proposed method can effectively reduce the copper loss of the machine. Hence, the above experimental results verified the effectiveness and superiority of the proposed method.

V. Conclusion

This article proposes an MTPA cooperative control strategy for a double stator DS-HEM considering inductance nonlinearity. The proposed DS-HEM can utilize the dc-bias current and consequent-pole PMs to achieve high torque density and good regulation capability. The current distribution of the proposed MTPA cooperative control strategy considering two dimensions of the armature current and dc-bias current is calculated by using the Lagrange extremum method. Moreover, the inductance nonlinearity is also considered by establishing the quadratic polynomial model. The output torque can be maximized by changing the proportion of the dc-bias component in the armature current. The experimental results verified the accuracy of the proposed nonlinear inductance model. Meanwhile, a prototype is fabricated and tested to validate the effectiveness of the proposed method. Compared with the only ac method and traditional method, the output torque of the proposed method has an increase of 42% and 14%, respectively.

References

[1] L. Qian, L. Sun, K. Wang, and M. Tong, "Fusion of position estimation techniques for a swing servo by a permanent-magnet synchronous machine," *IEEE Trans. Ind. Electron.*, vol. 70, no. 7, pp. 6551–6562, Jul. 2023.

[2] S. Wang et al., "Flux observer based on enhanced second-order generalized integrator with limit cycle oscillator for sensorless PMSM drives," *IEEE Trans. Power Electron.*, vol. 38, no. 12, pp. 15982–15995, Dec. 2023.

[3] J. Hang, H. Wu, S. Ding, Y. Huang, and W. Hua, "Improved loss minimization control for IPMSM using equivalent conversion method," *IEEE Trans. Power Electron.*, vol. 36, no. 2, pp. 1931–1940, Feb. 2021.

[4] J. Hang, M. Xia, S. Ding, Y. Li, L. Sun, and Q. Wang, "Research on vector control strategy of surface-mounted permanent magnet synchronous machine drive system with high-resistance connection," *IEEE Trans. Power Electron.*, vol. 35, no. 2, pp. 2023–2033, Feb. 2020.

[5] J. Jiang, S. Niu, and X. Zhang, "Torque improvement of a hybrid-excited vernier reluctance machine with high-order-harmonic winding design for electric vehicle application," *IEEE Trans. Transp. Electrific.*, vol. 10, no. 2, pp. 2397–2407, Jun. 2024.

[6] Z. Wu, L. Jin, W. Zhang, Y. Fan, W. Hua, and M. Cheng, "Influence of PWM excitation on DC winding induced voltage pulsation in wound field switched flux machines," *IEEE Trans. Ind. Appl.*, vol. 60, no. 1, pp. 460–476, Jan./Feb. 2024.

[7] F. Wei, Z. Q. Zhu, X. Sun, L. Yan, and J. Qi, "Investigation of asymmetric consequent-pole hybrid excited flux reversal machines," *IEEE Trans. Ind. Appl.*, vol. 58, no. 3, pp. 3434–3446, May 2022.

[8] Y. Fan, Y. Lei, and X. Wang, "An improved robust deadbeat predictive current control for the consequent-pole hybrid excitation motor," *IEEE Trans. Energy Convers.*, vol. 38, no. 2, pp. 1219–1230, Jun. 2023.

[9] L. Cinti, D. Michieletto, N. Bianchi, and M. Bertoluzzo, "Hybrid excited permanent magnet motor: Analytical sizing, finite element analysis and tests," *IEEE Trans. Ind. Appl.*, vol. 59, no. 6, pp. 6645–6654, Dec. 2023.

[10] S. Jia et al., "A high torque density concentrated winding vernier reluctance machine with DC-biased current," *IEEE Trans. Magn.*, vol. 54, no. 11, Nov. 2018, Art. no. 8205205.

[11] S. Jia, P. Chen, X. Dong, D. Liang, B. Li, and J. Liu, "Modeling and current control strategy for novel two-phase DC-biased vernier reluctance machine," *IEEE Trans. Ind. Appl.*, vol. 59, no. 1, pp. 814–822, Jan./Feb. 2023.

[12] Y. Meng, S. Fang, Z. Pan, and L. Qin, "A new hybrid-excited doubly salient dual-PM machine with DC-biased sinusoidal current," *IEEE Trans. Appl. Supercond.*, vol. 31, no. 8, Nov. 2021, Art. no. 5203205.

[13] G. Qu, J. Yu, Y. Liu, and W. Liu, "Design and analysis of a new consequent-pole hybrid excited permanent magnet machine with DC-biased current," in *Proc. IEEE Int. Magn. Conf. Short Papers*, 2024, pp. 1–2.

[14] T. Jiang, W. Zhao, and L. Xu, "Analysis of split-tooth stator PM vernier machines with zero-sequence current excitation," *IEEE Trans. Ind. Electron.*, vol. 70, no. 2, pp. 1229–1238, Feb. 2023.

[15] Y. Du, J. Zhao, F. Xiao, X. Zhu, L. Quan, and F. Li, "Partitioned stator hybrid excitation doubly salient machine with slot Halbach PM Arrays," *IEEE Trans. Veh. Technol.*, vol. 70, no. 4, pp. 3187–3196, Apr. 2021.

[16] Y. Du, Y. Mao, F. Xiao, X. Zhu, L. Quan, and F. Li, "Partitioned stator hybrid excited machine with DC-biased sinusoidal current," *IEEE Trans. Ind. Electron.*, vol. 69, no. 1, pp. 236–248, Jan. 2022.

[17] X. Gu, Z. Zhang, L. Sun, S. Yu, W. Zhang, and L. Yu, "Investigation of a parallel hybrid excitation machine with auxiliary winding for loss reduction in flux-weakening operation," *IEEE Trans. Transp. Electrific.*, vol. 10, no. 1, pp. 67–77, Mar. 2024.

[18] N. Pothi, Z. Q. Zhu, and Y. Ren, "Comparison of flux-weakening control strategies of novel hybrid-excited doubly salient synchronous machines," *IEEE Trans. Ind. Appl.*, vol. 55, no. 4, pp. 3589–3597, Aug. 2019.

[19] W. Ding and S. Li, "Maximum ratio of torque to copper loss control for hybrid excited flux-switching machine in whole speed range," *IEEE Trans. Ind. Electron.*, vol. 66, no. 2, pp. 932–943, Feb. 2019.

[20] X. Wang, Y. Fan, J. Chen, Y. Lei, Q. Chen, and C. H. T. Lee, "The current region control strategy with wide speed range of radial-axial consequent pole hybrid excitation machine for electric vehicles," *IEEE Trans. Transp. Electrific.*, vol. 10, no. 1, pp. 1377–1387, Mar. 2024.

[21] S. Jia, R. Qu, J. Li, D. Li, and W. Kong, "A stator-PM consequent-pole vernier machine with hybrid excitation and DC-biased sinusoidal current," *IEEE Trans. Magn.*, vol. 53, no. 6, Jun. 2017, Art. no. 8105404.

[22] X. Zhao, S. Niu, X. Zhang, and W. Fu, "A new relieving-DC-saturation hybrid excitation vernier machine for HEV starter generator application," *IEEE Trans. Ind. Electron.*, vol. 67, no. 8, pp. 6342–6353, Aug. 2020.

[23] Z. Q. Zhu, B. Lee, and X. Liu, "Integrated field and armature current control strategy for variable flux reluctance machine using open winding," *IEEE Trans. Ind. Appl.*, vol. 52, no. 2, pp. 1519–1529, Mar./Apr. 2016.

[24] Z. Yu, H. Gao, L. Chang, W. Kong, C. Gan, and R. Qu, "MTPA control strategy for six-phase DC-biased hybrid excitation vernier reluctance machines," in *Proc. IEEE Energy Convers. Congr. Expo.*, 2019, pp. 3807–3812.

[25] G. Liu, Z. Chen, L. Xu, T. Jiang, and L. Chang, "MTPA control for DC-biased hybrid excitation machine using MTPA control law and virtual signal injection," *IEEE Trans. Transp. Electrific.*, vol. 10, no. 1, pp. 1571–1582, Mar. 2024.

[26] X. Zhang, J. Zhao, Z. Yu, and Z. Pan, "Improved harmonic current injection control strategy for DC-biased-VRM based on current orthogonal component distribution to enhance output torque," *IEEE Trans. Power Electron.*, vol. 39, no. 10, pp. 12678–12689, Oct. 2024.

[27] J. Zhao, M. Lin, D. Xu, L. Hao, and W. Zhang, "Vector control of a hybrid axial field flux-switching permanent magnet machine based on particle swarm optimization," *IEEE Trans. Magn.*, vol. 51, no. 11, Nov. 2015, Art. no. 8204004.

[28] X. Lu, Y. Fan, and Y. Lei, "Efficiency-optimized control of new consequent-pole hybrid excitation motor," in *Proc. 24th Int. Conf. Elect. Mach. Syst.*, 2021, pp. 1702–1707.

[29] Q. Wang, S. Niu, and X. Luo, "A novel hybrid dual-PM machine excited by ac with DC bias for electric vehicle propulsion," *IEEE Trans. Ind. Electron.*, vol. 64, no. 9, pp. 6908–6919, Sep. 2017.

[30] Z. Q. Zhu and B. Lee, "Integrated field and armature current control for dual three-phase variable flux reluctance machine drives," *IEEE Trans. Energy Convers.*, vol. 32, no. 2, pp. 447–457, Jun. 2017.

[31] S. Jia, R. Qu, D. Li, J. Li, and W. Kong, "Improved torque capacity for flux modulated machines by injecting DC currents into the armature windings," *IEEE Trans. Magn.*, vol. 53, no. 6, Jun. 2017, Art. no. 8102205.

Han Yi received the B.S. degree in intelligent science and technology from Sun Yat-sen University, Shenzhen, China, in 2023. He is currently working toward the M.S. degree in electronic information with Sun Yat-Sen University, Shenzhen.

His research interests include the control strategy for hybrid excitation machines and the optimization design of permanent magnet machines.

Yiming Fan received the B.S. degree in intelligence science and technology from Sun Yat-sen University, Shenzhen, China, in 2024. He is currently working toward the M.S. degree in electronic information with Sun Yat-Sen University, Shenzhen.

His research interests include hybrid excitation machines, flux-modulated machines, and motor design and optimization.

Yuting Lu (Graduate Student Member, IEEE) received the B.S. degree in engineering from Sun Yat-sen University, Shenzhen, China, in 2023. He is currently working toward the M.S. degree in control science and engineering with the School of Intelligent Systems Engineering, Sun Yat-sen University, Shenzhen.

His research interests include modeling, optimization and control of electrical motors.

Guodong Feng (Senior Member, IEEE) received the B.S. and Ph.D. degrees in engineering from Sun Yat-sen University, Guangzhou, China, in 2010 and 2015, respectively.

From 2015 to 2019, he was a postdoctoral fellow with the University of Windsor, Windsor, ON, Canada. He is currently an Associate Professor at the School of Intelligent Systems Engineering, Sun Yat-sen University. His research interests include advanced signal processing, optimization, and electrical machines and drives.

Liangliang Wei (Member, IEEE) received the B.S. and Ph.D. degrees in electrical engineering from Wuhan University, Wuhan, China, in 2012 and 2017, respectively.

From 2017 to 2018, he was a postdoctoral researcher with Kyoto University, Kyoto, Japan, where he was engaged in permanent magnet machines. From 2018 to 2020, he was an Assistant Professor with Kyoto University. Since 2020, he has been an Associate Professor with the School of Intelligent Systems Engineering, Sun Yat-sen University, Shenzhen, China. His research interests include hybrid excitation machines, permanent magnet machines and drive control for electric vehicles, and state-of-health estimation for lithium-ion batteries.